Editors' Suggestion | Featured in Physics

Single-Enantiomer Spin Polarizers in Superconducting Junctions

Lorenz Meyer, Nicolas Néel, and Jörg Kröger*
Institut für Physik, Technische Universität Ilmenau, D-98693 Ilmenau, Germany

(Received 27 January 2026; accepted 21 April 2026; published 2 June 2026)

Decorating the superconducting Pb tip of a scanning tunneling microscope with a Mn atom cluster gives rise to Yu-Shiba-Rusinov resonances that serve as spin-sensitive probes of the tunneling current in junctions of single heptahelicene molecules adsorbed on Pb(111). The signal strength of these states in spectroscopy of the differential conductance depends on the handedness of the probed molecule, the direction of current flow, and the intramolecular site. These findings support the presence of the chirality-induced spin selectivity effect and the role of a single enantiomer as a spin polarizer.

DOI: 10.1103/pgs4-4nds

The chirality-induced spin selectivity (CISS) effect was first reported from photoelectron spectroscopy of Langmuir-Blodgett films [1], where a preferential photoelectron spin state was observed for a given chiral domain of the film. This pioneering work stimulated substantial experimental and theoretical studies, which have thoroughly been reviewed [2–4]. Despite its importance for fundamental physics and nanotechnological applications, the origin of the CISS effect, that is, the understanding of the chirality-induced locking of electron spin and momentum, is strongly debated and has remained elusive to date [5,6]. This dilemma is partly due to ambiguities in electron transport experiments involving chiral matter, which represent a major research direction devoted to the CISS effect. In these studies, chiral molecules are attached to ferromagnetic electrodes, and magnetoresistance has been reported as the response to chirality change or to reversing the magnetization of the ferromagnet [7–10]. With broken time-reversal symmetry due to an external magnetic field and in the linear electron transport regime, however, the claimed CISS effect is at odds with the Onsager-Casimir reciprocity relations [11–13]. Motivated by experimental observations [14–16], a work function change upon magnetization reversal has been proposed as an explanation to the magnetoresistive response of the junction [17]. Likewise, changes in the electric dipole of the chiral molecules can influence the CISS effect without altering the chirality [18–20]. The alarming consequence of these results is the open question as to whether single chiral molecules can act as spin polarizers at all. This intriguing incertitude has been fortified by a recent report on the apparent absence of the CISS effect in single-molecule break junctions [21].

The work presented here was stimulated by the unclear picture of the CISS effect at the single-molecule level. The studies were conceived in a manner that reduces the complexity to a minimum, retains the linear charge transport regime owing to low bias voltages, and avoids magnetization reversal. To this end, a racemic mixture of heptahelicene ($C_{30}H_{18}$, [7] H) molecules was adsorbed as a monomolecular layer on Pb(111) (see Supplemental Material [22]). The enantiomers Λ-[7] H and Δ-[7] H self-assemble in chiral domains and are clearly discriminated in scanning tunneling microscope (STM) images with intramolecular structure. Spin selectivity of electron transport across the enantiomer is probed via a superconducting Pb tip functionalized with a magnetic Mn cluster. The latter causes spin-polarized Yu-Shiba-Rusinov (YSR) states [23–25] within the Bardeen-Cooper-Schrieffer (BCS) energy gap [46] of the tip, which serve as probes for the spin polarization of the tunneling current and which circumvent the necessity of magnetization reversal. Exploring spectra of the differential conductance (dI/dV, where I is the current and V is the sample voltage) acquired atop the two chiral variants reveals a significant difference in the YSR signal strength. In addition, the identified dependence of the spectral signal on the current direction and on the intramolecular site favors the enantiomers acting as spin polarizers rather than as spin filters. These results evidence the single-enantiomer CISS effect at work.

Deposition of a racemic mixture of Λ-[7] H and Δ-[7] H on Pb(111) at room temperature gives rise to single-layer islands with an ordered molecular superstructure [Fig. 1(a)] that is incommensurate with the substrate lattice [22]. In contrast to observations from Cu(111) [47] and the (111) surfaces of Ag and Au [48,49], where zigzag rows of alternating enantiomers form, on Pb(111) the molecules

*Contact author: joerg.kroeger@tu-ilmenau.de

Published by the American Physical Society under the terms of the Creative Commons Attribution 4.0 International license. Further distribution of this work must maintain attribution to the author(s) and the published article's title, journal citation, and DOI.

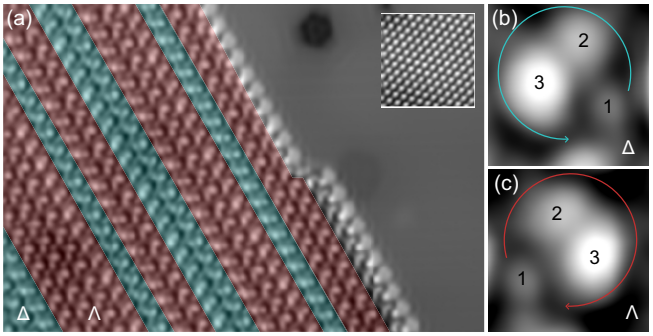


FIG. 1. (a) Constant-current STM image of a [7] H island with marked enantiopure domains (1 V, 50 pA, 30×20 nm). Inset: atomically resolved Pb(111) lattice (10 mV, 50 pA, 4×4 nm) (b), (c) STM images of a single (b) Δ and (c) Λ enantiomer embedded in a domain (1 V, 50 pA, 1.4×1.4 nm). Numbers 1–3 indicate an intramolecular pattern reflecting the helix with left (Λ) and right (Δ) handedness.

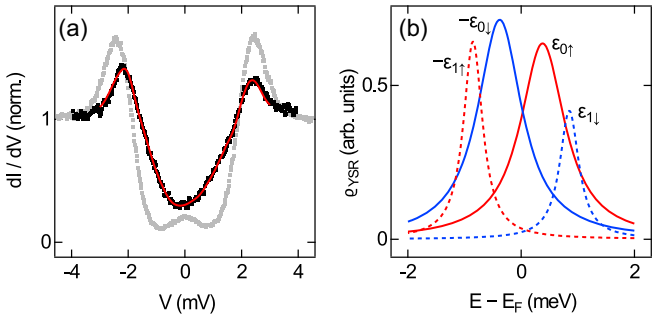


FIG. 2. (a) Spectra of dI/dV recorded with a clean (gray) and a Mn-terminated (black) tip atop clean Pb(111) at $T = 5$ K and in an external magnetic field of $B = 40$ mT. The solid line is a fit to the Mn tip spectrum [22]. Feedback loop parameters: 1 V, 50 pA. (b) Lorentzian density of states (ϱ_{YSR}) used for the fit in (a) ($\varepsilon_{i\sigma}$, YSR energy with respect to E_F, $i \in \{0, 1\}$, spin $\sigma \in \{\uparrow, \downarrow\}$).

arrange into straight enantiopure rows and domains, which with $\langle 1\bar{1}0 \rangle$ directions of the Pb(111) lattice subtend an angle of $(14 \pm 2)°$. On-surface chiral recognition of enantiomers as encountered here is known from early atomic force microscope studies of polymers [50].

It is essential to the interpretation of the spectroscopic findings to identify the enantiomers in STM images. The detailed view of individual enantiomers embedded in an island [Figs. 1(b) and 1(c)] serve this purpose. The spatial resolution enables the access to submolecular structure denoted as 1, 2, and 3, which is assigned to the charge density of the lowest unoccupied molecular orbital (LUMO) [22]. Such intramolecular resolution was best achieved at elevated voltages, which matches spectroscopy of dI/dV atop the enantiomers where signatures of the LUMO appear for $V \geq 1$ V [22]. The opposite sense of rotation toward increasing apparent height from 1 to 3 is evident for the two enantiomers. The resolution of intramolecular patterns does not only permit the unequivocal assignment of the enantiomer to the spectral quasielectron transport characteristics, it additionally allows one to explore possible variations of the enantioselective transmission at the atomic length scale. Both aspects will be discussed in the following.

To experimentally prove the electron spin polarization in charge transport across the enantiomers, a spin-sensitive probe is required, which is achieved by attaching a Mn cluster to the Pb tip. The termination of the tip with a Mn cluster proceeded via the indentation of the tip apex into an island of Mn atoms coadsorbed with the molecules [22] and was monitored by dI/dV spectra of the clean Pb(111) surface [Fig. 2(a)]. In the following, the spectra are normalized to their respective values at 5 mV. Normalization to an entire spectrum in the normal state yields virtually identical results (see Supplemental Material [22]). Deviating from the spectrum recorded with a clean Pb tip [gray dots in Fig. 2(a)] the spectrum acquired with the Mn-terminated tip exhibits asymmetrically positioned peaks at -2.26 and 2.35 mV (rather than at ± 2.44 mV resulting from spectra with a clean Pb tip). These spectral changes are attributed to the presence of intragap states. The experimental dI/dV data are best described [solid line in Fig. 2(a)] by assuming two pairs of YSR states represented each by two Lorentzians [22] at energies $\varepsilon_0 = \pm 0.38$ and $\varepsilon_1 = \pm 0.85$ meV [Fig. 2(b)]. While the opposite spin polarization of electron- and holelike components of YSR states is known [23–25,51,52], quantum fluctuations were demonstrated to diminish the spin polarization, which led to the suggested remedy of coupling the superconductor to a ferromagnet [53]. Indeed, the experimental verification of spin-polarized YSR states [52] as well as the use of YSR-functionalized tips as spin-active probes [54] were reported in an external magnetic field. Because of these precedent studies, an external magnetic field $B = 40$ mT $< B_c$ ($B_c = 42$ mT: critical field of Pb at 5 K [55]) was applied along the surface normal. However, the effect to be discussed next is likewise present in the case of $B = 0$, which demonstrates that the Mn cluster at the tip apex is large enough to stabilize its magnetic moment. Indeed, Mn clusters of as few as five atoms were shown to exhibit ferromagnetic order [56].

Figures 3(a) and 3(b) show the dI/dV spectra of the two enantiomers obtained atop site 3 with the same Mn-terminated Pb tip as used for the spectrum in Fig. 2(a). Remarkably, the spectra of Λ-[7] H and Δ-[7] H differ significantly [22]. At the feedback loop parameters used for spectroscopy, the apparent heights of Λ-[7] H and Δ-[7] H differ by less than 5 pm, which entails nearly the same tip-enantiomer distances and the exclusion of different tip stray fields at the molecular sites as a possible rationale to the enantiomer-specific spectra. The plots also include as gray dots molecule spectra acquired with a clean Pb tip. They are essentially indistinguishable from spectra of pristine Pb(111), which, importantly, shows that the adsorbed

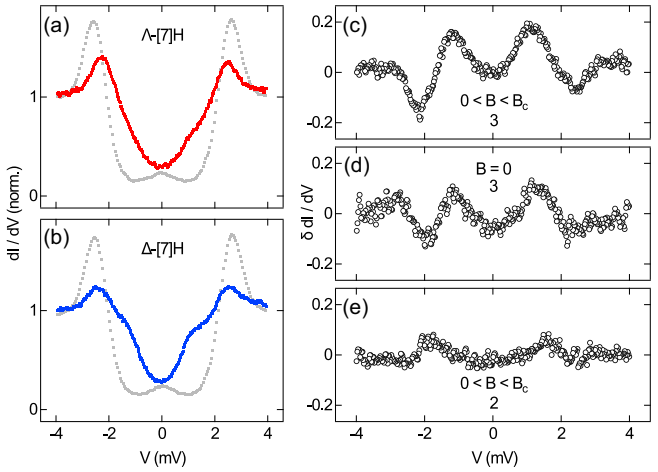


FIG. 3. (a),(b) Spectra of $\mathrm{d}I/\mathrm{d}V$ obtained at $B = 40$ mT with the same Mn-terminated tip as in Fig. 2(a) at site 3 of (a) Λ-[7] H and (b) Δ-[7] H. Gray dots depict spectroscopic data recorded with a clean Pb tip. Feedback loop parameters: 1 V, 50 pA. (c), (d) Difference spectra of (a), (b) at (c) $B = 40$ mT and (d) $B = 0$. (e) Difference spectrum obtained from $\mathrm{d}I/\mathrm{d}V$ data of Λ-[7] H and Δ-[7] H atop site 2.

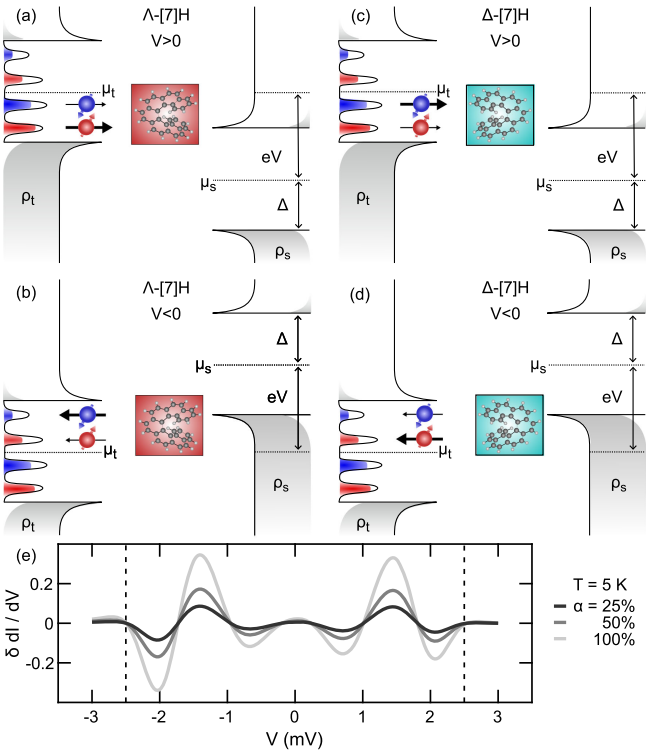


FIG. 4. (a) Left: tip DOS (ϱ_t) showing the BCS energy gap of width 2Δ for $T > 0$ and two pairs of spin-polarized YSR states. Right: sample DOS (ϱ_s). Quasielectron transport with indicated spin occurs from tip to sample due to positive sample voltage $V = (\mu_t - \mu_s)/e > 0$. (b) As (a) for $V < 0$. (c),(d) As (a),(b) for the Δ-[7] H enantiomer. The thickness of the horizontal arrows indicates the quasielectron transmission with the respective spin component. (e) Simulated $\delta\mathrm{d}I/\mathrm{d}V$ for $T = 5$ K with indicated polarization α ($\alpha = 100\%$ refers to the perfect transmission of quasielectrons with a single spin component). The dashed lines indicate the position of BCS gap edges in the case of a clean Pb-Pb tunneling junction.

enantiomers themselves do not induce intragap states, i.e., do not act as magnetic impurities. Consequently, different exchange coupling of the molecules to the Mn tip can likewise be excluded. In addition, a possible change in the order parameter of the conventional superconductor due to the presence of chiral molecules [57] is irrelevant.

Using now the experimental data for calculating the difference of spectral data, $\delta\mathrm{d}I/\mathrm{d}V = \mathrm{d}I_\Delta/\mathrm{d}V - \mathrm{d}I_\Lambda/\mathrm{d}V$, yields the evolution presented in Fig. 3(c) for $B = 40$ mT. In the field-free case [Fig. 3(d)], the excursions of $\delta\mathrm{d}I/\mathrm{d}V$ to positive and negative values are attenuated, but the general trend remains. For position 2, even in the case of applied field, the $\delta\mathrm{d}/\mathrm{d}V$ signal variations are essentially quenched. It is important to mention that for a given Mn-terminated tip $\delta\mathrm{d}I/\mathrm{d}V$ spectra are robust, i.e., they are reproducible for different pairs of enantiomers [22]. The structural integrity of the tip is controlled by intermediately recorded STM images and $\mathrm{d}I/\mathrm{d}V$ spectra of the clean surface. Changes of the tip inevitably lead to the interruption of the spectroscopy series and the preparation of a new tip. Previously, differences of $\mathrm{d}I/\mathrm{d}V$ spectra were likewise used to explore, e.g., the occurrence of YSR states [58] and the tunneling anisotropic magnetoresistance at the single-atom level [59]. These spectroscopic results are the main findings of the studies presented here. They demonstrate the CISS effect at the single-enantiomer level, as discussed next.

The interpretation of the data presented in Fig. 3 is depicted in Fig. 4. It illustrates the charge transport across enantiomers in the presence of superconducting electrodes and YSR states for the Λ enantiomer [Figs. 4(a) and 4(b)] and the Δ enantiomer [Figs. 4(c) and 4(d)]. The density of states (DOS) of the tip (ϱ_t) exhibits the BCS energy gap with symmetric flanks at $\mu_t \pm \Delta$ (μ_t, chemical potential of the tip; 2Δ, width of the BCS energy gap) together with two pairs of electron-hole-symmetric intragap states. Without loss of generality, the YSR state with high (low) binding energy ε_1 (ε_0) is assumed to exhibit spin-up (spin-down) polarization and the Λ enantiomer to preferentially transmit spin-up quasielectrons at positive sample voltage $V = (\mu_t - \mu_s)/e > 0$ (e, elementary charge), i.e., for quasielectron tunneling from the occupied YSR state to empty quasielectron states of the sample [Fig. 4(a)]. Reversing the bias voltage polarity entails the inversion of the current direction and, therefore, the preferential transmission of spin-down electrons from the sample to the unoccupied YSR state with spin-down polarization by the Λ enantiomer [Fig. 4(b)]. The opposite behavior applies to the Δ enantiomer [Figs. 4(c) and 4(d)] with spin-down and spin-up polarization of quasielectrons at, respectively, $V > 0$ and $V < 0$. Therefore, it is expected that the two

enantiomers interchange the signal strength among the two pairs of YSR states.

This picture of quasielectron transport was used to simulate the tunneling current across the enantiomers in the presence of the CISS effect [22]. Figure 4(e) shows the resulting $\delta \mathrm{d}I/\mathrm{d}V$ spectra. While different degrees of polarization were considered, the difference spectra are qualitatively similar. They exhibit pronounced minima close to the coherence peak positions (dashed lines) with $\delta \mathrm{d}I/\mathrm{d}V < 0$ and maxima inside the BCS energy gap with $\delta \mathrm{d}I/\mathrm{d}V > 0$. This evolution reflects the preferential transmission of quasielectrons by the Δ enantiomer to the low-energy (ε_0) pair of spin-polarized YSR states compared to the Λ enantiomer, whose transmission, in turn, is superior for the high-energy (ε_1) pair of YSR states with opposite spin polarization. Allowing in the simulations for reduced polarizations is seen to quench the $\delta \mathrm{d}I/\mathrm{d}V$ values. In particular, the variations of $\delta \mathrm{d}I/\mathrm{d}V$ close to $V = 0$ are attenuated. Importantly, the pairs of minima and maxima of $\delta \mathrm{d}I/\mathrm{d}V$ occur each at symmetric positive and negative voltages, as experimentally observed.

The good agreement of experimental [Figs. 3(c)–3(e)] and simulated [Fig. 4(e)] $\delta \mathrm{d}I/\mathrm{d}V$ traces corroborates the dependence of the CISS effect on the current direction and, therefore, qualifies the enantiomers as spin polarizers rather than as spin filters [60]. Additionally, it is conjectured here that the spin polarization is generated within the respective enantiomer alone. A spin polarization of the substrate electron DOS caused by the interaction with the adsorbed chiral molecules [26] can be excluded because the symmetry in $\delta \mathrm{d}I/\mathrm{d}V$ traces [Figs. 3(c) and 3(d)] contrasts the quasielectron transport behavior expected from a spin-polarized substrate electron DOS and the concomitant magnetoresistance of the junction [22]. Furthermore, the spatially resolved spectroscopy experiments unveiled that the extent of the CISS effect depends on the actual site of the enantiomer, which is evidenced by $\delta \mathrm{d}I/\mathrm{d}V \approx 0$ obtained at position 2 in the relevant voltage range [Fig. 3(e)]. Because 2 is apparently lower than 3, where the maximum effect is observed, the result in Fig. 3(e) reflects the previously reported dependence of the spin polarization on the length of the chiral molecule [61–64]. The spatial variability of the CISS effect likewise offers an explanation to the null result in recent break junction experiments [21], where the lacking spatial resolution requires the averaging over a multitude of current-voltage characteristics obtained from contacts without direct access to the molecule orientation. It is likewise noteworthy that the voltages involved in the spectroscopies are on the order of 1 mV, which supports the assumption of the linear electron transport regime.

Additional experiments were performed to exclude, e.g., a possible dependence of the effect on the enantiomer adsorption site. Because of the incommensurate adsorption structure, adjacent molecules of the same enantiopure domain occupy different sites of the Pb(111) surface and may therefore exhibit different spectra. However, spectra of adjacent molecules in an enantiopure domain are essentially identical [22]. Another important aspect is the exclusion of electrostatic effects in the observations. To this end, the spectra of the molecules were explored for different tip-enantiomer distances [22]. The presence of the tip locally modifies the surface potential with implications on band bending and work function changes [17], as well as on molecular electric dipoles [18–20]. Because the spectra remain invariant for varying tip-molecule separations, such effects are considered irrelevant here. Finally, a possible influence of spin-orbit coupling (SOC) due to the presence of Pb is addressed because the enantiomers could then take the role of orbital filters, which would entail spin filtering due to SOC in the metal electrodes [65]. Calculations of the Pb bulk band structure with and without SOC [66,67] unveiled, however, that the strongest SOC-induced changes occur for bands with energies far above the Fermi level at wave vector $k = 0$. In addition, SOC affects bands at and close to E_F only for elevated k. These findings for bulk Pb are in agreement with more recent experimental and simulated band structure data for Pb(111) [68]. The results therefore substantiate the irrelevance of SOC in the present spectroscopy experiments, where quasielectron transport is studied in the vicinity of E_F and where tunneling with $k \neq 0$ is exponentially suppressed.

While the reliable interpretation of the experimental data relies on the difference spectra and, thus, on the invariance of the tip structural integrity in spectroscopy atop various enantiomers, different Mn-terminated tips with different YSR resonance textures were independently prepared in order to verify the robustness of the CISS effect. Expectedly [23–25,27–31], the different tips gave rise to altered YSR states that yielded modified $\delta \mathrm{d}I/\mathrm{d}V$ data. However, the basic trend of $\delta \mathrm{d}I/\mathrm{d}V$, i.e., the occurrence of pairs of maxima and pairs of minima at symmetric positive and negative voltages [Figs. 3(c)–3(e)], which is indicative of the CISS effect, was retained [22].

In conclusion, the use of spin-polarized YSR states as probes for the quasielectron spin state circumvents the reversal of electrode magnetization and unambiguously evidences the dependence of the superconducting STM junction conductance on the handedness of the probed chiral molecule in the linear transport regime. Because of the additionally broken time-reversal symmetry, the Onsager-Casimir reciprocity relations appear to fail for chiral molecules in metal electrode junctions [69]. The reported experimental approach further excludes electrostatic effects, such as work function changes or electric-dipole modifications, to feign the CISS effect. The dependence of the spin-selective quasielectron transport on the current direction and on the intramolecular site demonstrates the spin polarizer behavior of the individual enantiomers. Based on the presented findings, reinforced

theoretical efforts in understanding the single-enantiomer CISS effect that possibly include the revisiting of the symmetry considerations in the Onsager-Casimir reciprocity relations are anticipated. Moreover, the simple model system character allows for artificial atomic-scale modifications of the enantiomer environment, such as the presence of magnetic impurities or quantum-confined electron states, which will further help understand the CISS effect at the ultimate size.

Acknowledgments—Discussions with Bart van Wees, Krisztián Palotás, Pius Theiler, Maximilian Kögler, and Karl Rothe are appreciated. Funding by the Deutsche Forschungsgemeinschaft (Grant No. KR 2912/21-1), the Agence Nationale de la Recherche (Grant No. ANR-23-CE09-0036-01), and the German Federal Ministry of Education and Research within the "Forschungslabore Mikroelektronik Deutschland (ForLab)" initiative is acknowledged.

Data availability—The data that support the findings of this article are not publicly available upon publication because it is not technically feasible and/or the cost of preparing, depositing, and hosting the data would be prohibitive within the terms of this research project. The data are available from the authors upon reasonable request.

[1] K. Ray, S. P. Ananthavel, D. H. Waldeck, and R. Naaman, Asymmetric scattering of polarized electrons by organized organic films of chiral molecules, Science **283**, 814 (1999).
[2] B. P. Bloom, Y. Paltiel, R. Naaman, and D. H. Waldeck, Chiral induced spin selectivity, Chem. Rev. **124**, 1950 (2024).
[3] R. Naaman, Y. Paltiel, and D. H. Waldeck, Chiral molecules and the electron spin, Nat. Rev. Chem. **3**, 250 (2019).
[4] X. Wang, X. Li, Y. He, Z. Xu, H. Pan, J. Li, Y. Wang, W. Dong, H. Chen, Q. Shen, Z. Shen, S. Hou, K. Wu, Y. Zhang, and Y. Wang, Chirality induced spin selectivity in electron transport investigated by scanning probe microscopy, J. Phys. **37**, 113003 (2025).
[5] F. Evers, R. Korytár, S. Tewari, and J. M. van Ruitenbeek, Advances and challenges in single-molecule electron transport, Rev. Mod. Phys. **92**, 035001 (2020).
[6] S. Sarkar, A. Sharoni, O. L. A. Monti, and Y. Dubi, The spinterface mechanism for the chiral-induced spin selectivity effect: A critical perspective, ACS Nano **19**, 37484 (2025).
[7] S. Mishra, A. K. Mondal, E. Z. B. Smolinsky, R. Naaman, K. Maeda, T. Nishimura, T. Taniguchi, T. Yoshida, K. Takayama, and E. Yashima, Spin filtering along chiral polymers, Angew. Chem., Int. Ed. Engl. **59**, 14671 (2020).
[8] A. K. Mondal, M. D. Preuss, M. L. Ślęczkowski, T. K. Das, G. Vantomme, E. W. Meijer, and R. Naaman, Spin filtering in supramolecular polymers assembled from achiral monomers mediated by chiral solvents, J. Am. Chem. Soc. **143**, 7189 (2021).
[9] R. Malatong, T. Sato, J. Kumsampao, T. Minato, M. Suda, V. Promarak, and H. M. Yamamoto, Highly durable spin filter switching based on self-assembled chiral molecular motor, Small **19**, 2302714 (2023).
[10] M. R. Safari, F. Matthes, C. M. Schneider, K.-H. Ernst, and D. E. Bürgler, Spin-selective electron transport through single chiral molecules, Small **20**, 2308233 (2024).
[11] L. Onsager, Reciprocal relations in irreversible processes. I., Phys. Rev. **37**, 405 (1931).
[12] L. Onsager, Reciprocal relations in irreversible processes. II., Phys. Rev. **38**, 2265 (1931).
[13] H. B. G. Casimir, On Onsager's principle of microscopic reversibility, Rev. Mod. Phys. **17**, 343 (1945).
[14] J. M. Abendroth, K. M. Cheung, D. M. Stemer, M. S. El Hadri, C. Zhao, E. E. Fullerton, and P. S. Weiss, Spin-dependent ionization of chiral molecular films, J. Am. Chem. Soc. **141**, 3863 (2019).
[15] S. Ghosh, S. Mishra, E. Avigad, B. P. Bloom, L. T. Baczewski, S. Yochelis, Y. Paltiel, R. Naaman, and D. H. Waldeck, Effect of chiral molecules on the electron's spin wavefunction at interfaces, J. Phys. Chem. Lett. **11**, 1550 (2020).
[16] P. M. Theiler, C. Ritz, R. Hofmann, and A. Stemmer, Detection of a chirality-induced spin selective quantum capacitance in α-helical peptides, Nano Lett. **23**, 8280 (2023).
[17] S. H. Tirion and B. J. van Wees, Mechanism for electrostatically generated magnetoresistance in chiral systems without spin-dependent transport, ACS Nano **18**, 6028 (2024).
[18] M. Eckshtain-Levi, E. Capua, S. Refaely-Abramson, S. Sarkar, Y. Gavrilov, S. P. Mathew, Y. Paltiel, Y. Levy, L. Kronik, and R. Naaman, Cold denaturation induces inversion of dipole and spin transfer in chiral peptide monolayers, Nat. Commun. **7**, 10744 (2016).
[19] T. N. H. Nguyen, G. Salvan, O. Hellwig, Y. Paltiel, L. T. Baczewski, and C. Tegenkamp, The mechanism of the molecular CISS effect in chiral nano-junctions, Chem. Sci. **15**, 14905 (2024).
[20] A. C. Aragonès, M. Varese, K. Garg, W. Kuang, Q. Wang, E. Giralt, V. Mujica, R. Gutierrez, G. Cuniberti, L. Puerta, and I. Díez-Pérez, Dipole-induced inversion of spin-dependent charge transport through α-helical peptide-based single-molecule junctions, J. Am. Chem. Soc. **147**, 36453 (2025).
[21] L. Li, W. Shi, A. Mahajan, J. Zhang, M. Gómez-Gómez, J. Labella, S. Louie, T. Torres, S. Barlow, S. R. Marder, D. R. Reichman, and L. Venkataraman, Too fast for spin flipping: Absence of chirality-induced spin selectivity in coherent electron transport through single-molecule junctions, J. Am. Chem. Soc. **147**, 25043 (2025).
[22] See Supplemental Material at http://link.aps.org/supplemental/10.1103/pgs4-4nds for experimental methods, adsorption of [7]H, orbital texture of the enantiomers, normalization of differential-conductance spectra, CISS effect for different tips, simulation of the tunneling current, comparison of enantiomer and substrate spectra, tunneling magnetoresistance versus CISS effect, CISS effect and the enantiomer adsorption site, CISS effect and tip-enantiomer distance, which includes Refs. [17,20,23–45].

[23] L. Yu, Bound state in superconductors with paramagnetic impurities, Acta Phys. Sin. **21**, 75 (1965).
[24] H. Shiba, Classical spins in superconductors, Prog. Theor. Phys. **40**, 435 (1968).
[25] A. I. Rusinov, Superconductivity near a paramagnetic impurity, JETP Lett. **9**, 85 (1969).
[26] H. Alpern, K. Yavilberg, T. Dvir, N. Sukenik, M. Klang, S. Yochelis, H. Cohen, E. Grosfeld, H. Steinberg, Y. Paltiel, and O. Millo, Magnetic-related states and order parameter induced in a conventional superconductor by nonmagnetic chiral molecules, Nano Lett. **19**, 5167 (2019).
[27] K. J. Franke, G. Schulze, and J. I. Pascual, Competition of superconducting phenomena and Kondo screening at the nanoscale, Science **332**, 940 (2011).
[28] M. Ruby, Y. Peng, F. von Oppen, B. W. Heinrich, and K. J. Franke, Orbital picture of Yu-Shiba-Rusinov multiplets, Phys. Rev. Lett. **117**, 186801 (2016).
[29] D.-J. Choi, C. Rubio-Verdú, J. de Bruijckere, M. M. Ugeda, N. Lorente, and J. I. Pascual, Mapping the orbital structure of impurity bound states in a superconductor, Nat. Commun. **8**, 15175 (2017).
[30] S. Amann, N. Kucska, A. Lászlóffy, N. Néel, B. Újfalussy, L. Rózsa, K. Palotás, and J. Kröger, Magnetic bound states of iron clusters on a superconductor, Phys. Rev. B **108**, 195403 (2023).
[31] B. Noßmann, Z. Yu, A. Das, S. Schulte, N. Néel, C.-T. Wu, S. Kirchner, and J. Kröger, Yu–Shiba–Rusinov states induced by single Fe atoms on reconstructed compound superconductor V_3Si, Surf. Sci. **746**, 122504 (2024).
[32] L. Limot, J. Kröger, R. Berndt, A. Garcia-Lekue, and W. A. Hofer, Atom transfer and single-adatom contacts, Phys. Rev. Lett. **94**, 126102 (2005).
[33] J. Kröger, N. Néel, and L. Limot, Contact to single atoms and molecules with the tip of a scanning tunnelling microscope, J. Phys. **20**, 223001 (2008).
[34] I. Horcas, R. Fernández, J. M. Gómez-Rodríguez, J. Colchero, J. Gómez-Herrero, and A. M. Baro, WSXM: A software for scanning probe microscopy and a tool for nanotechnology, Rev. Sci. Instrum. **78**, 013705 (2007).
[35] M. Safari, F. Matthes, K.-H. Ernst, D. Bürgler, and C. Schneider, Deposition of chiral heptahelicene molecules on ferromagnetic Co and Fe thin-film substrates, Nanomater. Nanotechnol. **12**, 3281 (2022).
[36] C. Lee, W. Yang, and R. G. Parr, Development of the Colle-Salvetti correlation-energy formula into a functional of the electron density, Phys. Rev. B **37**, 785 (1988).
[37] A. D. Becke, Density-functional exchange-energy approximation with correct asymptotic behavior, Phys. Rev. A **38**, 3098 (1988).
[38] M. Kettner, V. V. Maslyuk, D. Nürenberg, J. Seibel, R. Gutierrez, G. Cuniberti, K.-H. Ernst, and H. Zacharias, Chirality-dependent electron spin filtering by molecular monolayers of helicenes, J. Phys. Chem. Lett. **9**, 2025 (2018).
[39] Gaussian ~16 Revision C.01 (2016), gaussian Inc. Wallingford CT.
[40] R. Dennington, T. A. Keith, and J. M. Millam, Gaussview Version 6 (2019), semichem Inc. Shawnee Mission KS.
[41] M. Ruby, F. Pientka, Y. Peng, F. von Oppen, B. W. Heinrich, and K. J. Franke, Tunneling processes into localized subgap states in superconductors, Phys. Rev. Lett. **115**, 087001 (2015).
[42] R. C. Dynes, V. Narayanamurti, and J. P. Garno, Direct measurement of quasiparticle-lifetime broadening in a strong-coupled superconductor, Phys. Rev. Lett. **41**, 1509 (1978).
[43] M. Bode, Spin-polarized scanning tunnelling microscopy, Rep. Prog. Phys. **66**, 523 (2003).
[44] R. Wiesendanger, Spin mapping at the nanoscale and atomic scale, Rev. Mod. Phys. **81**, 1495 (2009).
[45] M. Julliere, Tunneling between ferromagnetic films, Phys. Lett. **54A**, 225 (1975).
[46] J. Bardeen, L. N. Cooper, and J. R. Schrieffer, Theory of superconductivity, Phys. Rev. **108**, 1175 (1957).
[47] M. Parschau, R. Fasel, and K.-H. Ernst, Coverage and enantiomeric excess dependent enantiomorphism in two-dimensional molecular crystals, Cryst. Growth Des. **8**, 1890 (2008).
[48] J. Seibel, M. Parschau, and K.-H. Ernst, Two-dimensional crystallization of enantiopure and racemic heptahelicene on Ag(111) and Au(111), J. Phys. Chem. C **118**, 29135 (2014).
[49] J. Seibel, M. Parschau, and K.-H. Ernst, Double layer crystallization of heptahelicene on noble metal surfaces, Chirality **32**, 975 (2020).
[50] R. Viswanathan, J. A. Zasadzinski, and D. K. Schwartz, Spontaneous chiral symmetry breaking by achiral molecules in a Langmuir–Blodgett film, Nature (London) **368**, 440 (1994).
[51] A. V. Balatsky, I. Vekhter, and J.-X. Zhu, Impurity-induced states in conventional and unconventional superconductors, Rev. Mod. Phys. **78**, 373 (2006).
[52] L. Cornils, A. Kamlapure, L. Zhou, S. Pradhan, A. A. Khajetoorians, J. Fransson, J. Wiebe, and R. Wiesendanger, Spin-resolved spectroscopy of the Yu-Shiba-Rusinov states of individual atoms, Phys. Rev. Lett. **119**, 197002 (2017).
[53] A. Skurativska, J. Ortuzar, D. Bercioux, F. S. Bergeret, and M. A. Cazalilla, Robust spin polarization of Yu-Shiba-Rusinov states in superconductor/ferromagnetic insulator heterostructures, Phys. Rev. B **107**, 224507 (2023).
[54] L. Schneider, P. Beck, J. Wiebe, and R. Wiesendanger, Atomic-scale spin-polarization maps using functionalized superconducting probes, Sci. Adv. **7**, eabd7302 (2021).
[55] J. Eisenstein, Superconducting elements, Rev. Mod. Phys. **26**, 277 (1954).
[56] R. J. Van Zee, C. A. Baumann, S. V. Bhat, and J. Weltner, W., ESR of the high-spin ($S = 25/2$) Mn_5 molecule, J. Chem. Phys. **76**, 5636 (1982).
[57] H. Alpern, E. Katzir, S. Yochelis, N. Katz, Y. Paltiel, and O. Millo, Unconventional superconductivity induced in Nb films by adsorbed chiral molecules, New J. Phys. **18**, 113048 (2016).
[58] A. Yazdani, B. A. Jones, C. P. Lutz, M. F. Crommie, and D. M. Eigler, Probing the local effects of magnetic impurities on superconductivity, Science **275**, 1767 (1997).
[59] N. Néel, S. Schröder, N. Ruppelt, P. Ferriani, J. Kröger, R. Berndt, and S. Heinze, Tunneling anisotropic magnetoresistance at the single-atom limit, Phys. Rev. Lett. **110**, 037202 (2013).

[60] J. Lee, S.-H. Lee, U. Jeong, D. J. C. Dalayoan, S. Shin, H. Y. Jeong, H. Jin, B. Yan, N. Park, and S. Namgung, Real space imaging of spin scattering in chirality-induced spin selectivity, ACS Nano **19**, 42046 (2025).

[61] K. Senthil Kumar, N. Kantor-Uriel, S. P. Mathew, R. Guliamov, and R. Naaman, A device for measuring spin selectivity in electron transfer, Phys. Chem. Chem. Phys. **15**, 18357 (2013).

[62] M. Kettner, B. Göhler, H. Zacharias, D. Mishra, V. Kiran, R. Naaman, D. H. Waldeck, S. Sęk, J. Pawłowski, and J. Juhaniewicz, Spin filtering in electron transport through chiral oligopeptides, J. Phys. Chem. C **119**, 14542 (2015).

[63] K. B. Ghosh, W. Zhang, F. Tassinari, Y. Mastai, O. Lidor-Shalev, R. Naaman, P. Möllers, D. Nürenberg, H. Zacharias, J. Wei, E. Wierzbinski, and D. H. Waldeck, Controlling chemical selectivity in electrocatalysis with chiral CuO-coated electrodes, J. Phys. Chem. C **123**, 3024 (2019).

[64] A. Ghazaryan, Y. Paltiel, and M. Lemeshko, Analytic model of chiral-induced spin selectivity, J. Phys. Chem. C **124**, 11716 (2020).

[65] Y. Liu, J. Xiao, J. Koo, and B. Yan, Chirality-driven topological electronic structure of DNA-like materials, Nat. Mater. **20**, 638 (2021).

[66] X. Zubizarreta, V. M. Silkin, and E. V. Chulkov, First-principles quasiparticle damping rates in bulk lead, Phys. Rev. B **84**, 115144 (2011).

[67] C. Tresca, G. Profeta, G. Marini, G. B. Bachelet, A. Sanna, M. Calandra, and L. Boeri, Why mercury is a superconductor, Phys. Rev. B **106**, L180501 (2022).

[68] W.-C. Chen, C.-H. Chen, A. Huang, K. Lei, D. Mikolas, M.-k. Dai, J.-M. Kuo, D.-S. Lin, C.-M. Cheng, H.-T. Jeng, and S.-J. Tang, Formation of surface states on Pb(111) by Au adsorption, Sci. Rep. **13**, 1689 (2023).

[69] J. Fransson, Breaking of time-reversal symmetry and onsager reciprocity in chiral molecule interfaced with an environment, APL Comput. Phys. **2**, 016111 (2026).